Influence of Unwanted First-Order Sideband on Optical Vector Analysis Based on Optical Single-Sideband Modulation

Min Xue and Shilong Pan, *Senior Member, IEEE, Member, OSA*

***Abstract*—Optical vector analyzer (OVA) based on optical single-sideband (OSSB) modulation is attractive due to its potential sub-Hz resolution. However, the accuracy and dynamic range are limited by the unwanted sidebands of the OSSB signal, including the high-order sidebands and the unwanted first-order sideband. Previously, the influence of the high-order sidebands has been studied and several methods to suppress the errors induced by the high-order sidebands have been proposed. However, the investigation of the influence of the unwanted first-order sideband is still insufficient. In this paper, an analytical model is established and a numerical simulation is performed to comprehensively study the impact of the unwanted first-order sideband on the accuracy and dynamic range of the OSSB-based OVA. Then the simulation results are verified by experiment, which indicates that the unwanted first-order sideband has evident influence on the measurement accuracy and places a restriction on the dynamic range. Given that some prior information of the transmission responses is known, certain parameters of the device under test may still be achievable with high accuracy even when large unwanted first-order sideband is presented. This study may provide guidance in design and application of the OSSB-based OVA.**

***Index Terms*—Measurement techniques, microwave photonics, optical modulation, optical variables measurement, optical vector analyzer.**

I. Introduction

OPTICAL devices having the capability of manipulating the optical spectrum with a resolution of sub-MHz or higher are highly desired in emerging applications such as label-free detection down to single molecules [1], optical storage based on slow-light [2], [3], on-chip optical signal processing [4] and so on. Measuring the magnitude and phase responses is essential for their fabrication and application. Optical vector analysis is such a technology to simultaneously acquire the magnitude and phase responses of optical devices, by which other key parameters such as dispersion, group delay (GD), polarization dependent loss (PDL), polarization mode dispersion (PMD) and so on, can be further calculated. Previously, optical vector analyzers (OVAs) were constructed based on modulation phase-shift approach [5] or interferometry approach [6]. In these OVAs, the spectral responses are extracted by scanning the wavelength of a laser source. Restricted by the low wavelength stability of the wavelength-swept laser source, the resolution is usual >1.6 pm (i.e. 200 MHz @ 1550 nm), so that the spectral responses of optical devices with MHz-level or less fine structure cannot be characterized.

To achieve high-resolution measurement, OVAs based on optical single-sideband (OSSB) modulation have been proposed [7]. Thanks to the high-fineness microwave frequency sweeping and high-accuracy phase-magnitude detection, the OSSB-based OVA can potentially achieve sub-Hz resolution [8] and was demonstrated to have 78-kHz resolution in an experiment [9]. However, the undesired sidebands in the OSSB signal, including the high-order sidebands induced by the nonlinearity of the electro-optic modulators (EOMs) and the residual unwanted first-order sideband, place a restriction on the measurement accuracy and dynamic range of the magnitude, phase, and polarization responses [10]. The influence of the high-order sidebands on the measurement accuracy and the dynamic range was investigated [11], and approaches to suppress the high-order-sideband induced errors were proposed [12]–[16], by which the accuracy and the dynamic range of the OSSB-based OVA are significantly improved. In addition, a model of the OVA based on a 90-degree electrical hybrid coupler and a dual-drive Mach-Zehnder modulator was built, by which a study on the influence of the sideband suppression ratio (SSR) of the OSSB signal on the measurement accuracy was given [17]. The results show that the measured magnitude and phase responses get more accurate with the increase of the SSR. To eliminate the measurement error induced by the unwanted first-order sideband, two approaches were developed [18], [19]. However, it still lacks a comprehensive study on the influence of the unwanted first-order sideband, which is essential to estimate the accuracy and dynamic range of the implemented OSSB-based OVA.

In this paper, analytical analysis, numerical simulation and experiment are employed to comprehensively investigate the influence of the unwanted first-order sideband on the measurement accuracy and the dynamic range of the OSSB-based OVA. Given that the high-order-sideband induced errors are ignorable in a small index case, a general analytical model for studying

Manuscript received January 26, 2017; revised March 23, 2017 and April 11, 2017; accepted April 13, 2017. Date of publication April 17, 2017; date of current version May 15, 2017. This work was supported in part by the National Natural Science Foundation of China under Grants 61527820 and 61422108, in part by the Jiangsu Provincial Program for High-level Talents in Six Areas (DZXX-034), and the "333 Project" of Jiangsu Province (BRA2015343). *(Corresponding author: Shilong Pan.)*

The authors are with the Key Laboratory of Radar Imaging and Microwave Photonics, Nanjing University of Aeronautics and Astronautics, Nanjing 211106, China (e-mail: xuemin@nuaa.edu.cn; pans@ieee.org).

Color versions of one or more of the figures in this paper are available online at http://ieeexplore.ieee.org.

Digital Object Identifier 10.1109/JLT.2017.2695221

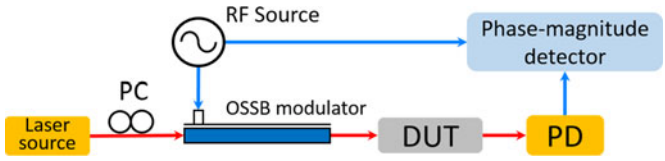

Fig. 1. The schematic diagram of the basic OSSB-based OVA. PC: polarization controller, OSSB: optical single-sideband, DUT: device under test, PD: photodetector.

the influence of the residual −1st-order sideband is established. Then, a numerical simulation and an experiment are performed. The results show that the unwanted −1st-order sideband has evident influence on the measurement accuracy and dynamic range, which decreases with the SSR of the OSSB signal. The phase of the unwanted −1st-order sideband also has significant influence on the measured results even at the same SSR. In addition, if some prior information of the transmission responses is known, certain parameters of the device under test (DUT) may still be achievable with high accuracy even when large unwanted first-order sideband is existed.

II. Analytical Analysis

Fig. 1 shows the schematic diagram of the basic OSSB-based OVA. In the scheme, the most important component is the OSSB modulator, which can be realized by a dual-drive EOM or two cascaded EOMs together with a 90-degree/120-degree electrical hybrid coupler [12], [20], a double-sideband modulator and an optical filter to remove one sideband [9], [21], and a double-sideband modulator followed by an optical Hilbert transformer [22]. Different schemes would produce OSSB signals with different relationships between the desired +1st-order sideband and the unwanted −1st-order sideband. To be general, we denote the OSSB signal as

$$E_{\text{in}}(\omega) = A_{-1}\cdot\delta\left[\omega-(\omega_o-\omega_e)\right] + A_0\cdot\delta(\omega-\omega_o) + A_{+1}\cdot\delta\left[\omega-(\omega_o+\omega_e)\right] \quad (1)$$

where ω_{o} and ω_{e} are the angular frequencies of the optical carrier and the RF signal, respectively, and A_{-1}, A_0 and A_{+1} are the complex amplitudes of the unwanted −1st-order sideband, the optical carrier and the desired +1st-order sideband. The high-order sidebands are ignored by assuming a small modulation index case.

The generated OSSB signal goes through an optical DUT, in which the magnitude and phase of the optical carrier and the two first-order sidebands are changed according to the transmission function of the DUT. Thereby, the optical signal carries the spectral responses, which can be expressed as

$$E_{\text{out}}(\omega) = A_{-1}H(\omega_o-\omega_e)\cdot\delta\left[\omega-(\omega_o-\omega_e)\right] + A_0H(\omega_o)\cdot\delta(\omega-\omega_o) + A_{+1}H(\omega_o+\omega_e)\cdot\delta\left[\omega-(\omega_o+\omega_e)\right] \quad (2)$$

where $H(\omega)=H_{\text{DUT}}(\omega)\cdot H_{\text{sys}}(\omega)$, $H_{\text{DUT}}(\omega)$ and $H_{\text{sys}}(\omega)$ are the transmission functions of the DUT and the measurement system, respectively. A photodetector (PD) is followed to convert the optical signal into a photocurrent. The phase-magnitude detector only extracts the magnitude and phase of the ω_{e}-component in the photocurrent, which is

$$i(\omega_e) = \eta A_{+1}A_0^*H(\omega_o+\omega_e)H^*(\omega_o) + \eta A_0A_{-1}^*H(\omega_o)H^*(\omega_o-\omega_e) \quad (3)$$

where η is the responsivity of the PD. At the right hand of (3), the first term is the component carrying the spectral responses of the DUT, and the second term is the measurement error introduced by the unwanted −1st-order sideband.

To achieve $H_{\text{sys}}(\omega)$, a calibration step, which is implemented by directly connecting the two test ports, i.e. $H_{\text{DUT}}(\omega)=1$, has to be performed. In this case, the photocurrent is given by

$$i_{\text{cal}}(\omega_e) = \eta A_{+1}A_0^*H_{\text{sys}}(\omega_o+\omega_e)H_{\text{sys}}^*(\omega_o) + \eta A_0A_{-1}^*H(\omega_o)_{\text{sys}}H_{\text{sys}}^*(\omega_o-\omega_e) \quad (4)$$

From (3) and (4), the transmission function of the DUT is obtained, shown in (5) at the bottom of this page, where

$$\text{SSR}\cdot\exp(i\Delta\varphi) = \frac{A_{+1}A_0^*}{A_0A_{-1}^*} \quad (6)$$

$H_{\text{DUT}}^*(\omega_o)$ is the transmission function of the DUT at ω_{o} which is measurable complex constant, $\text{SSR}=|A_{+1}|/|A_{-1}|$, and $\Delta\varphi$ is the phase difference between the beat note of the +1st-order sideband and the optical carrier and that of the −1st-order sideband and the optical carrier in the OSSB signal.

As can be seen from (5), the measurement error is dependent highly on the feature of the OSSB-signal generator, and the spectral responses of the measurement system and the DUT. In addition, the selection of ω_{o} would also affect the measurement error. It should be noted that in practice one would concern more about the ratio of the measurement error and the actual response. When $H_{\text{DUT}}(\omega)$ becomes small, this ratio would grow. In some extreme case (e.g. at the deep notch), the accurate magnitude and phase might be submerged by the measurement error. Thus, the dynamic range of the OSSB-based OVA would be restricted

$$\begin{aligned} H_m(\omega_o+\omega_e) &= \frac{i(\omega_e)}{i_{\text{cal}}(\omega_e)H_{\text{DUT}}^*(\omega_o)} \\ &= \frac{A_{+1}A_0^*H(\omega_o+\omega_e)H^*(\omega_o)+A_0A_{-1}^*H(\omega_o)H^*(\omega_o-\omega_e)}{\left[A_{+1}A_0^*H_{\text{sys}}(\omega_o+\omega_e)H_{\text{sys}}^*(\omega_o)+A_0A_{-1}^*H(\omega_o)_{\text{sys}}H_{\text{sys}}^*(\omega_o-\omega_e)\right]H_{\text{DUT}}^*(\omega_o)} \\ &= \frac{\text{SSR}\cdot\exp(i\Delta\varphi)H(\omega_o+\omega_e)H^*(\omega_o)+H(\omega_o)H^*(\omega_o-\omega_e)}{\left[\text{SSR}\cdot\exp(i\Delta\varphi)H_{\text{sys}}(\omega_o+\omega_e)H_{\text{sys}}^*(\omega_o)+H(\omega_o)_{\text{sys}}H_{\text{sys}}^*(\omega_o-\omega_e)\right]H_{\text{DUT}}^*(\omega_o)} \end{aligned} \quad (5)$$

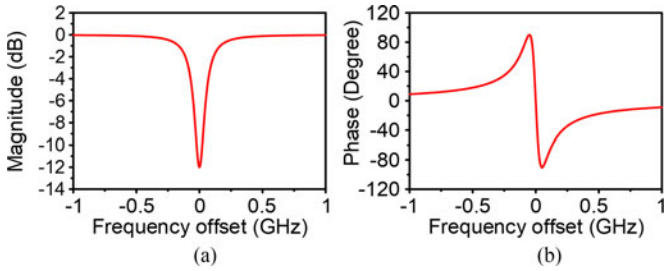

Fig. 2. The magnitude and phase responses of the FBG under test.

by the unwanted −1st-order sideband. The phase of the unwanted −1st-order sideband would also have significant impact on the measured spectral responses since the measured spectral responses are the vectorial sum of the actual responses and the measurement error.

It is worth mentioning that the influence of the responses of the measurement system is small and ignorable, since the spectral responses of the measurement system on the both sides of the optical carrier are generally symmetrical and have small ripple with the wavelength.

III. Numerical Simulation

In order to comprehensively understand the influence of the unwanted first-order sideband in the OSSB signal on the measurement accuracy and the dynamic range of the OSSB-based OVA, a numerical simulation is performed. In the simulation, the transmission function of the measurement system is assumed to be $H_{\rm sys}(\omega) = 1$, so (5) can be rewritten as (7) shown at the bottom of this page. In practice, the optical DUT that can manipulate optical spectrum with an ultrahigh resolution always has a deep notch in transmission response, which is symmetrical to the notch center [1]–[4]. Therefore, in the simulation an ideal fiber Bragg grating (FBG) with magnitude and phase responses shown in Fig. 2 is served as the optical DUT, which has a notch depth of 12 dB, a 3-dB bandwidth of 173.2 MHz and a phase shift of 180°.

A. Magnitude Response

From (3), the photocurrent at the output port of the PD is the vectorial sum of E_{+1} and E_{-1}, where E_{+1} (or E_{-1}) is the component beaten by the +1st-order (or −1st-order) sideband and the optical carrier after the DUT. The phase difference of E_{+1} and E_{-1} is the sum of $\Delta\varphi$ and the phase difference of the frequency response of the DUT at the two wavelengths. Therefore, the range of the magnitude of the photocurrent in the PD is

$$|E_{+1}| - |E_{-1}| \le |E_{+1} + E_{-1}| \le |E_{+1}| + |E_{-1}| \qquad (8)$$

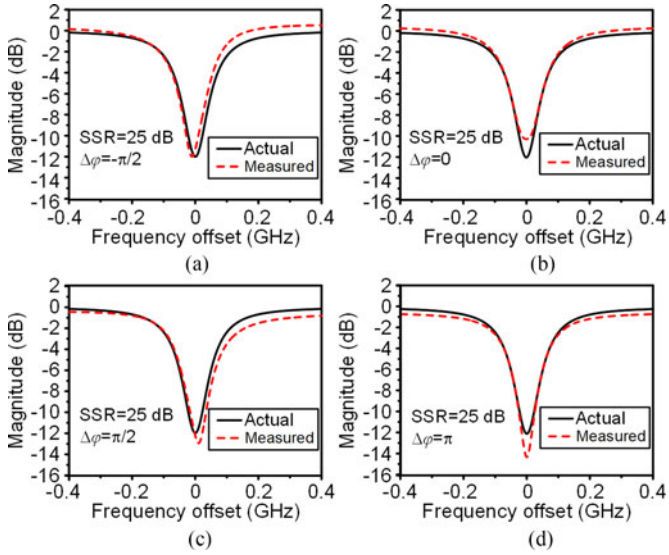

Fig. 3. The magnitude responses measured with different $\Delta\varphi$ in simulation when the SSR of the OSSB signal is 25 dB.

Fig. 3 shows the magnitude responses of the FBG measured by the OSSB-based OVA with different $\Delta\varphi$ in simulation when the SSR of the OSSB signal is 25 dB. As can be seen, the measured magnitude responses are different for different $\Delta\varphi$, which agrees with the analytical analysis.

For an optical DUT that can manipulate optical spectrum with an ultrahigh resolution, notch depth, center frequency and 3-dB bandwidth are the most interesting parameters, which can be achieved from the measured magnitude response. The notch depth describes the suppression of the DUT on the optical signal, while the center frequency and the 3-dB bandwidth respectively indicate the working frequency and bandwidth of the DUT. Since the phase response of the FBG at the center of the notch is 0 and the phase response at the unwanted first-order sideband approach 0, as can be seen from Fig. 2(b), the phase difference of E_{+1} and E_{-1} approaches to $\Delta\varphi$ when measuring the notch depth and the center frequency. In addition, 3-dB bandwidth is also dependent on $\Delta\varphi$ because the shape of the frequency response varies with $\Delta\varphi$, as can be seen in Fig. 3.

Fig. 4(a) shows the measured notch depth of the FBG with the SSR and the $\Delta\varphi$ of the OSSB signal. As can be seen from Fig. 4(a), the measured notch depth approaches the actual one with the increase of the SSR, and the measurement error changes according to $\Delta\varphi$ for a fixed SSR. When E_{+1} and E_{-1} are in phase, the magnitude of the photocurrent equals to the maximal value (i.e. $|E_{+1}| + |E_{-1}|$). As a result, the measured notch depth is minimal. When E_{+1} and E_{-1} are out of phase, the magnitude of the photocurrent equals to the minimal value (i.e. $|E_{+1}| - |E_{-1}|$), leading to the maximal notch depth. In other cases, the measured notch depth is between the minimal and

$$\begin{aligned} H_m(\omega_o + \omega_e) &= \frac{\mathrm{SSR}\cdot\exp(i\Delta\varphi)\,H_{\rm DUT}(\omega_o+\omega_e)\,H^*_{\rm DUT}(\omega_o) + H_{\rm DUT}(\omega_o)\,H^*_{\rm DUT}(\omega_o-\omega_e)}{[\mathrm{SSR}\cdot\exp(i\Delta\varphi)+1]\,H^*_{\rm DUT}(\omega_o)} \\ &= \frac{\mathrm{SSR}\cdot\exp(i\Delta\varphi)}{\mathrm{SSR}\cdot\exp(i\Delta\varphi)+1}H_{\rm DUT}(\omega_o+\omega_e) + \frac{H_{\rm DUT}(\omega_o)\,H^*_{\rm DUT}(\omega_o-\omega_e)}{[\mathrm{SSR}\cdot\exp(i\Delta\varphi)+1]\,H^*_{\rm DUT}(\omega_o)} \end{aligned} \qquad (7)$$

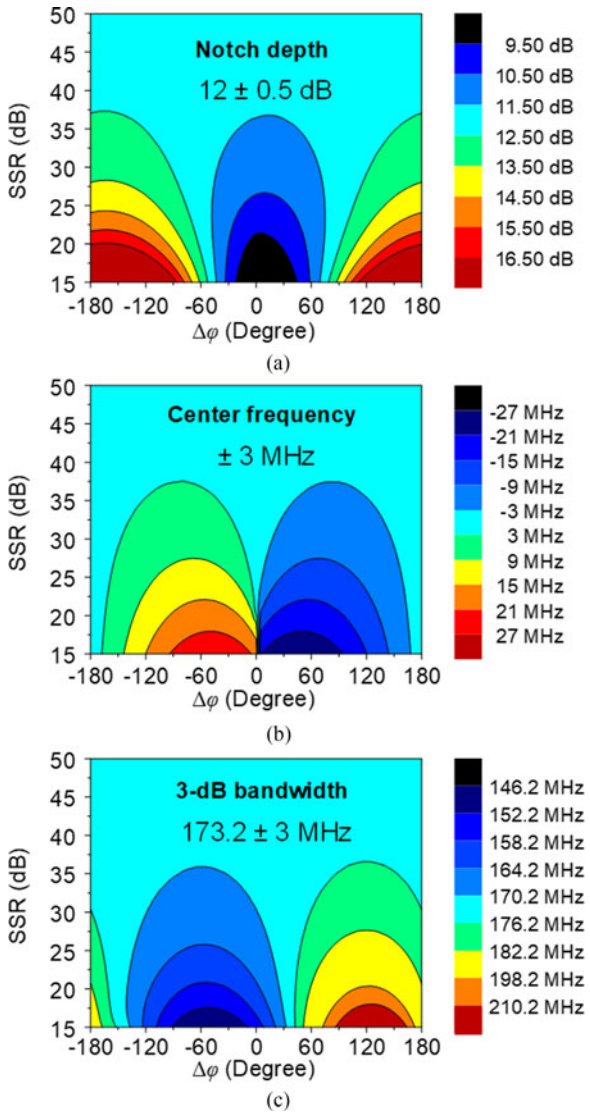

Fig. 4. The influence of the unwanted −1st-order sideband on the measured (a) notch depth, (b) center frequency and (c) 3-dB bandwidth

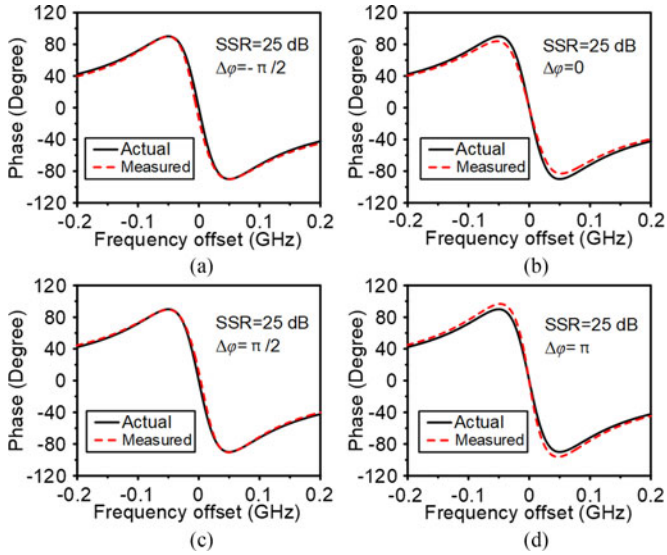

Fig. 5. The phase responses measured with different $\Delta\varphi$ in simulation when the SSR of the OSSB signal is 25 dB.

maximal values. It should be noted that the maximal notch-depth measurement error is not exactly present at $\Delta\varphi = 0$ or π in the measurement since the phase difference of E_{+1} and E_{-1} is determined by both of $\Delta\varphi$ and the transmission response of the DUT.

Fig. 4(b) shows the impact of the unwanted -1st-order sideband including the SSR and $\Delta\varphi$ on the center frequency measurement. When E_{+1} and E_{-1} are in phase or out of phase, the magnitude measurement error is symmetrical to the center frequency and therefore the center frequency can be accurately identified. Nevertheless, for other cases, the measured results would contain asymmetrical measurement error, leading to center-frequency measurement error. This error decreases with the increase of the SSR of the OSSB signal. For instance, the maximal measurement error can reach 17.91 MHz when the SSR of the OSSB signal is 20 dB, and decrease to 2.25 MHz if the SSR of the OSSB signal increases to 40 dB. For the label-free detection based on the optical resonators [1], the improvement on the center frequency measurement could enhance the sensing accuracy of the sensors, making the molecule having a smaller diameter detectable. It should be noted that the maximal center-frequency measurement error is not present at a predictable $\Delta\varphi$ in the measurement due to the influenced of the transmission response of the DUT on the phase difference of E_{+1} and E_{-1}.

Fig. 4(c) shows the influence of the unwanted -1st-order sideband on the measured 3-dB bandwidth. When measuring the 3-dB bandwidth, not only the magnitude of the $+1$st-order sideband is suppressed by 3 dB, but also the phase is obviously shifted. Hence, the measured 3-dB bandwidth changes according to $\Delta\varphi$ when the SSR of the OSSB signal is fixed. Again, the measured 3-dB bandwidth approaches the actual one with the growth of the SSR. The maximum bandwidth measurement error is 15.26% when the SSR is 20 dB and 1.15% if the SSR is 40 dB.

From above analysis, to achieve accurate notch depth, center frequency and 3-dB bandwidth of the narrow notch filters, the SSR of the OSSB signal should be as large as possible. Then, $\Delta\varphi$ can be set to be 0 or π to measure the accurate center frequency.

B. Phase Response

From (3), if E_{+1} and E_{-1} are in phase or out of phase, there is no phase measurement error, while large phase error is presented when E_{+1} and E_{-1} are quadrature (i.e. having a phase difference of $\pm$ 90 degree). Since the phase difference of E_{+1} and E_{-1} is the sum of $\Delta\varphi$ and the phase difference of the frequency response of the FBG at the two wavelengths, the phase measurement errors are different for different $\Delta\varphi$ and different actual phases.

Fig. 5 shows the phase responses of the FBG measured by an OSSB signal with a SSR of 25 dB when applying different $\Delta\varphi$ in simulation. Because the FBG has a maximal phase of $\pi/2$ and

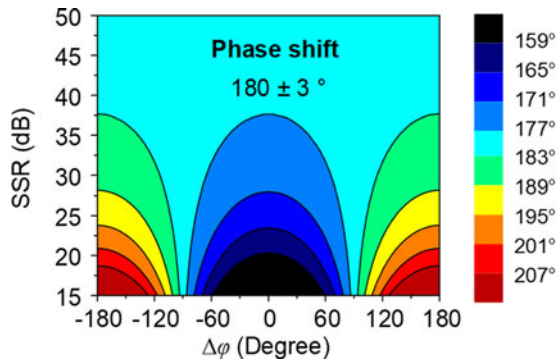

Fig. 6. The influence of the unwanted −1st-order sideband on the measured phase shift.

a minimal phase of $-\pi/2$, E_{+1} and E_{-1} have phase differences of 0 and -π at the two extreme points when $\Delta\varphi = -\pi/2$. Therefore, the unwanted first-order sideband does not introduce any phase error, as shown in Fig. 5(a). Around the center frequency, however, the measured phases contain obvious measurement errors since the +1st-order sideband is greatly suppressed by the deep notch (i.e. the power of E_{+1} is comparable with that of E_{-1}) and the phase difference of E_{+1} and E_{-1} is $-\pi/2$. Similarly, for $\Delta\varphi = \pi/2$, the phase differences between E_{+1} and E_{-1} are respectively π and 0 when measuring the maximal and minimal phases, so the maximal phase shift of the FBG can be accurately obtained, as shown in Fig. 5(c). At frequencies around the center frequency, the measured phases are smaller because E_{+1} and E_{-1} have comparable powers and the phase of E_{-1} is smaller than that of E_{+1}. When $\Delta\varphi = 0$ or π, E_{+1} and E_{-1} have a phase difference of π/2 (or -π/2) when measuring the maximal (or minimal) phase response. In this case, the measurement error of the phase shift of the FBG can reach 13°, as shown in Fig. 5(b) and (c). It is worth noting that the measured phase responses at the notch center is accurate since the actual phase is 0 and E_{+1} and E_{-1} are in phase or out of phase.

To investigate the influence of the unwanted −1st-order sideband on measuring the phase shift, which is an interesting parameter for narrow-bandwidth notch filter, another simulation is performed with the results shown in Fig. 6. As can be seen, the measured phase shift approaches the actual one with the increase of the SSR. As the change of $\Delta\varphi$, the errors in the measured phase shift rise and fall accordingly. For a fixed SSR, when $\Delta\varphi = -\pi/2$ or $\pi/2$, the measured phase shifts at SSRs always equal to the actual ones, and when $\Delta\varphi = 0$ or π, the measurement error is the largest, reaching 12.93% for SSR = 20 dB, and 1.27% for SSR = 40 dB.

In previous measurement systems, $\Delta\varphi$ is not controlled since it is determined by both of the OSSB signal and the transmission function of the measurement system, so it is important to evaluate the maximal measurement errors at different SSRs when $\Delta\varphi$ is varied from -π to π. Table I shows the calculated results for an optical DUT with a notch depth of 12 dB, a 3-dB bandwidth of 173.2 MHz and a phase shift of 180°. As can be seen, the measurement errors are non-ignorable when the SSR of the OSSB signal is smaller than 50 dB. It should be mentioned that the measurement accuracy of the notch depth depends not only the SSR and $\Delta\varphi$ but also the responses of the DUT. For fixed SSR and $\Delta\varphi$, the accuracy decreases with the notch depth.

TABLE I
THE MAXIMAL MEASUREMENT ERROR WHEN $\Delta\varphi$ IS NOT CONTROLLED

SSR (dB)	Notch depth	Center Frequency (MHz)	3-dB bandwidth	Phase shift
15	91.40 %	25.89	39.62 %	22.91 %
20	38.12 %	17.91	15.26 %	12.93 %
30	10.10 %	6.89	3.85 %	4.05 %
40	3.04 %	2.25	1.15 %	1.27 %
50	0.95 %	0.72	0.36 %	0.40 %

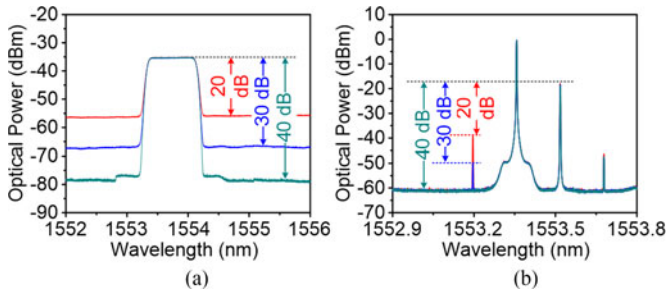

Fig. 7. (a) The optical filter shapes of the WaveShaper and (b) the optical spectra of the OSSB signals with different SSRs.

IV. EXPERIMENTAL RESULTS

In order to verify the analytical analysis and the numerical simulation, an experiment is carried out, in which the magnitude and phase responses of a FBG are measured at different SSRs when $\Delta\varphi = 0$ and π.

In the experiment, the OSSB-based OVA shown in Fig. 1 is constructed. A tunable laser source (TLS, Agilent N7714A) is used to provide the optical carrier, which is modulated by a RF signal from an electrical vector network analyzer (VNA, R&S ZVA67) at an OSSB modulator. The OSSB modulator is comprised of an EOM and a programmable optical filter (Finisar, WaveShaper 4000 s) which can form an optical filter with different shapes. To make $\Delta\varphi = 0$, the EOM is implemented by a single-drive Mach-Zehnder modulator (MZM, Fujitsu FTM7938EZ) biased at the quadrature transmission point (QTP), which is stabilized by a modulator bias controller (MBC, YYLabs Inc.); and to let $\Delta\varphi = \pi$ a phase modulator (PM, EOSpace Inc.) is applied. A FBG written on a polarization maintaining fiber is used as an optical DUT. A 50-GHz PD (Finisar XPD2150R) is inserted to convert the optical signal into a photocurrent. The phase-magnitude detector in the VNA extracts the magnitude and phase of the photocurrent. The optical spectra of the modulated signals are monitored by an optical spectrum analyzer (OSA, Finisar WaveAnalyzer 1500S) with a resolution of 150 MHz.

Fig. 7 shows the shapes of the bandpass optical filter implemented by the WaveShaper and the optical spectra of the OSSB signals with different SSRs. As can be seen, OSSB signals with SSRs of 20 dB, 30 dB and 40 dB are respectively generated by filtering the optical double-sideband (ODSB)

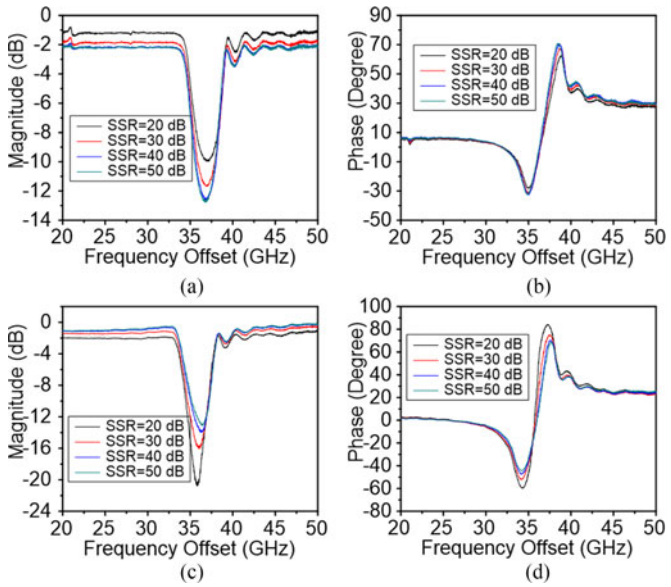

Fig. 8. The magnitude and phase responses measured by (a), (b) the MZM-based OSSB signal, and (c), (d) the PM-based OSSB signal.

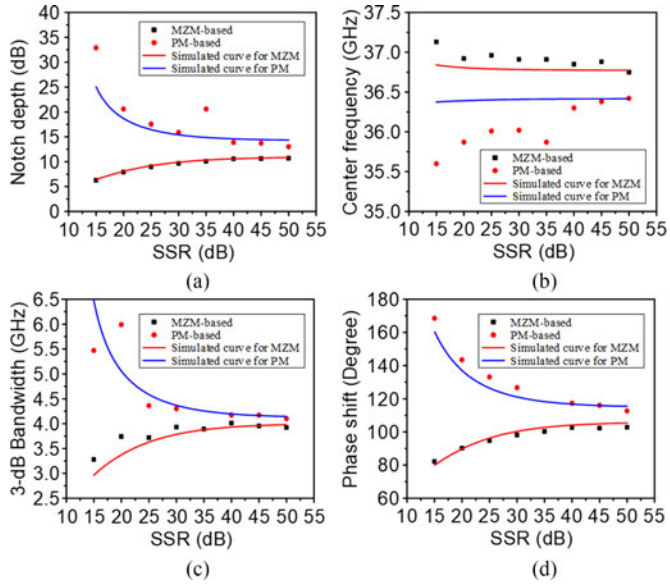

Fig. 9. The experimentally measured (a) notch depth, (b) center frequency, (c) 3-dB bandwidth, and (d) phase shift when applying the MZM-based and PM-based OSSB signals with difference SSRs.

signal produced by the MZM or the PM via the WaveShaper. The EOMs work in a small modulation index case, so the powers of the second-order sidebands are much smaller than those of the optical carrier and the $+1$st-order sidebands, making the influence of the second-order sidebands ignorable.

Fig. 8 shows the magnitude and phase responses of the FBG measured with the MZM-based OSSB signal or the PM-based OSSB signal. As can be seen, with the growth of the SSR, the measured magnitude and phase responses converge in both cases. According to the simulation in Section III, we refer the limit values at infinite SSR to the actual responses thereafter. Since the polarization-maintaining FBG is sensitive to the polarization of the OSSB signals while the polarizations of the PM-based and MZM-based OSSB signals are different due to their non-polarization maintaining pigtails, the magnitude and phase responses of the FBG in two cases have some difference. It should be noted the ripples in Fig. 8 are the natural responses of the FBG.

When the MZM is biased at the QTP (i.e. $\Delta\varphi = 0$), the measured spectral responses are generally larger than the actual ones, as shown in Fig. 8(a) and (b). For the measured magnitude responses, the largest errors appear at the notch center where E_{+1} and E_{-1} have the same phase and the smallest power difference. Increasing the SSR of the OSSB signal, the power difference between E_{+1} and E_{-1} grows and the error induced by E_{-1} reduces. As a result, the measured magnitude responses as well as the measured phase responses get accurate, as shown in Fig. 8(a) and (b). On the other hand, when the PM is applied (i.e. $\Delta\varphi = \pi$), the measured spectral responses are smaller than the actual one, as shown in Fig. 8(c) and (d). The largest measurement errors also appears when measuring the notch center, due to the smallest power difference and the opposite phase of E_{+1} and E_{-1}. With the increase of the SSR, the measured magnitude and phase responses approach the actual ones.

TABLE II
THE KEY PARAMETERS OF THE FBGS IN SIMULATION

	Notch depth (dB)	Center Frequency (GHz)	3-dB bandwidth (GHz)	Phase shift (Degree)
$\Delta\varphi = 0$	10.70	36.75	3.93	102.85
$\Delta\varphi = \pi$	13.02	36.42	4.09	112.63

Fig. 9 shows the notch depth, center frequency, 3-dB bandwidth and phase shift of the FBG measured by the MZM-based and PM-based OSSB signals with different SSRs in the experiment. The simulated curves in the cases of $\Delta\varphi = 0$ and π are also plotted for comparison. Due to the dissimilar responses of the polarization-maintaining FBG in two measurements, the key parameters of the FBGs in the simulation are different, as shown in Table II.

As can be seen, with the increase of the SSR, the measured notch depth, center frequency, 3-dB bandwidth and phase shift approach the actual ones. For the notch depth, 3-dB bandwidth and the phase shift measurement, the simulation results are verified by the experimentally measured results. It should be mentioned that the simulation results in Fig 9(b) indicate that the center frequency can be accurately obtained when $\Delta\varphi = 0$ or π. However, in the experiment, the measured center frequencies contain the measurement errors, since the phase response of the measurement system would introduce extra phase difference between E_{+1} and E_{-1}. As a result, E_{+1} and E_{-1} are not exactly in phase or out phase, so the measured center frequencies still contains obvious errors.

V. CONCLUSIONS AND DISCUSSION

In conclusion, the influence of the unwanted first-order sideband in the OSSB signal on the measurement accuracy and

the dynamic range of the OSSB-based OVA was theoretically, numerically and experimentally investigated. The results show that the unwanted −1st-order sideband introduces considerable measurement errors in the magnitude and phase responses measurement and restricts the dynamic range of the OSSB-based OVA. The influence deceases with the SSR of the OSSB signal. Hence, to improve the accuracy and the dynamic range of the OSSB-based OVA, the unwanted −1st-order sideband should be well suppressed.

REFERENCES

[1] F. Vollmer and S. Arnold, "Whispering-gallery-mode biosensing: label-free detection down to single molecules," *Nature Methods*, vol. 5, pp. 591–596, 2008.

[2] L. Liu *et al.*, "An ultra-small, low-power, all-optical flip-flop memory on a silicon chip," *Nature Photon.*, vol. 4, no. 3, pp. 182–187, 2010.

[3] E. Karimi and R. W. Boyd, "Ten years of nature Physics: Slowly but surely," *Nat. Phys.*, vol. 11, no. 1, pp. 15–16, 2015.

[4] W. S. Fegadolli, L. Feng, M. M.-U. Rahman, J. E. Oliveira, V. R. Almeida, and A. Scherer, "Experimental demonstration of a reconfigurable silicon thermo-optical device based on spectral tuning of ring resonators for optical signal processing," *Opt. Express*, vol. 22, no. 3, pp. 3425–3431, 2014.

[5] T. Niemi, M. Uusimaa, and H. Ludvigsen, "Limitations of phase-shift method in measuring dense group delay ripple of fiber bragg gratings," *IEEE Photon. Technol. Lett.*, vol. 13, no. 12, pp. 1334–1336, Dec. 2001.

[6] D. M. Baney and B. Szafraniec, "Elementary matrix method for dispersion analysis in optical systems," *J. Lightw. Tech.*, vol. 28, no. 4, pp. 294–307, Feb. 2010.

[7] S. L. Pan and M. Xue, "Ultrahigh-resolution optical vector analysis based on optical single-sideband modulation," *IEEE/OSA J. Lightw. Tech.*, vol. 35, no. 4, pp. 836–845, Feb. 2017, doi: 10.1109/JLT.2016.2598477.

[8] J. E. Román, M. Y. Frankel, and R. D. Esman, "Spectral characterization of fiber gratings with high resolution," *Opt. Lett.*, vol. 23, no. 12, pp. 939–941, 1998.

[9] Z. Z. Tang, S. L. Pan, and J. P. Yao, "A high resolution optical vector network analyzer based on a wideband and wavelength-tunable optical single-sideband modulator," *Opt. Express*, vol. 20, no. 6, pp. 6555–6560, 2012.

[10] M. Sagues, M. Pérez, and A. Loayssa, "Measurement of polarization dependent loss, polarization mode dispersion and group delay of optical components using swept optical single sideband modulated signals," *Opt. Express*, vol. 16, no. 20, pp. 16181–16188, 2008.

[11] M. Xue, S. L. Pan, X. W. Gu, and Y. J. Zhao, "Performance analysis of optical vector analyzer based on optical single-sideband modulation," *J. Opt. Soc. Amer. B*, vol. 30, no. 4, pp. 928–933, 2013.

[12] M. Xue, S. L. Pan, and Y. J. Zhao, "Optical single-sideband modulation based on a dual-drive MZM and a 120-degree hybrid coupler," *J. Lightw. Tech.*, vol. 32, no. 19, pp. 3317–3323, Oct. 2014.

[13] M. Xue, S. L. Pan, and Y. J. Zhao, "Accuracy improvement of optical vector network analyzer based on single-sideband modulation," *Opt. Lett.*, vol. 39, no. 12, pp. 3595–3598, 2014.

[14] W. T. Wang, W. Li, J. G. Liu, W. H. Sun, W. Y. Wang, and N. H. Zhu, "Optical vector network analyzer with improved accuracy based on Brillouin-assisted optical carrier processing," *IEEE Photon. J.*, vol. 6, no. 6, pp. 1–10, Dec. 2014.

[15] M. Xue, S. L. Pan, and Y. J. Zhao, "Accurate optical vector network analyzer based on optical single-sideband modulation and balanced photodetection," *Opt. Lett.*, vol. 40. no. 4, pp. 569–572, 2015.

[16] W. Li, W. H. Sun, W. T. Wang, L. X. Wang, J. G. Liu, and Z. N. Hua, "Reduction of measurement error of optical vector network analyzer based on DPMZM," *IEEE Photon. Technol. Lett.*, vol. 26, no. 9, pp. 866–869, May 2014.

[17] R. Hernández, A. Loayssa, and D. Benito, "Optical vector network analysis based on single-sideband modulation," *Opt. Eng.*, vol. 43, no. 10, pp. 2418–2421, 2004.

[18] M. Wang and J. P. Yao, "Optical vector network analyzer based on unbalanced double-sideband modulation," *IEEE Photon. Technol. Lett.*, vol. 25, no. 8, pp. 753–755, Apr. 2013.

[19] M. Xue, S. L. Pan, and Y. J. Zhao, "Large dynamic range optical vector analyzer based on optical single-sideband modulation and Hilbert transform," *Appl. Phys. B, Laser Opt.*, vol. 122, no. 7, p. 197, Jul. 2016.

[20] Y. M. Zhang, F. Z. Zhang, and S. L. Pan, "Optical single sideband modulation with tunable optical Carrier-to-Sideband ratio," *IEEE Photon.Tech. Lett.*, vol. 26, no. 7, pp. 653–655, Apr. 2014.

[21] S. R. Blais and J. P. Yao, "Optical single sideband modulation using an ultranarrow dual-transmission-band fiber Bragg grating," *IEEE Photon. Technol. Lett.*, vol. 18, no. 21, pp. 2230–2232, Nov. 2006.

[22] Z. Li, H. Chi, X. Zhang, and J. P. Yao, "Optical single-sideband modulation using a Fiber-Bragg-Grating-Based optical Hilbert transformer," *IEEE Photon. Technol. Lett.*, vol. 23, no. 9, pp. 558–560, May 2011.

Min Xue was born in Changzhou, China, in September 1988. He received the B.S. and Ph.D. degrees from the College of Electronic and Information Engineering, Nanjing University of Aeronautics and Astronautics, Nanjing, China, in 2011 and 2016, respectively. He joined the College of Electronic and Information Engineering, Nanjing University of Aeronautics and Astronautics, in 2016, where he is currently a member of the Key Laboratory of Radar Imaging and Microwave Photonics. His research interests include photonic microwave measurement and metrology, optical fiber sensor, and integrated microwave photonics.

Shilong Pan (S'06–M'09–SM'13) received the B.S. and Ph.D. degrees in electronics engineering from Tsinghua University, Beijing, China, in 2004 and 2008, respectively.

From 2008 to 2010, he was a "Vision 2010" Postdoctoral Research Fellow in the Microwave Photonics Research Laboratory, University of Ottawa, Ottawa, ON, Canada. In 2010, he joined the College of Electronic and Information Engineering, Nanjing University of Aeronautics and Astronautics, Nanjing, China, in 2010, where he is currently a Full Professor and the Executive Director of the Key Laboratory of Radar Imaging and Microwave Photonics. He has authored or coauthored more than 270 research papers, including more than 140 papers in peer-reviewed journals and 130 papers in conference proceedings. His research interest focuses on microwave photonics, which includes optical generation and processing of microwave signals, analog photonic links, photonic microwave measurement, and integrated microwave photonics.

Prof. Pan is a Senior Member of the IEEE Microwave Theory and Techniques Society, the IEEE Photonics Society and a member of the Optical Society of America. He received an OSA Outstanding Reviewer Award in 2015. He was the Chair of numerous international conferences and workshops, including the TPC Chair of the International Conference on Optical Communications and Networks in 2015, the TPC Co-Chair of the IEEE International Topical Meeting on Microwave Photonics in 2017, the TPC Chair of the High-Speed And Broadband Wireless Technologies Subcommittee of the IEEE Radio Wireless Symposium in 2013, 2014, and 2016, respectively, the TPC Chair of the Optical Fiber Sensors And Microwave Photonics Subcommittee of the OptoElectronics and Communication Conference in 2015, and the Chair of the Microwave Photonics For Broadband Measurement Workshop of International Microwave Symposium in 2015.